Available online at www.sciencedirect.com

ScienceDirect

Ceramics International 39 (2013) 9627–9635

CERAMICS INTERNATIONAL

www.elsevier.com/locate/ceramint

Structural, optical and microwave dielectric properties of $Sr_{1-x}Ca_xWO_4$ ceramics prepared by the solid state reaction route

Nidhi Khobragade[a], Ela Sinha[a], S.K. Rout[a,*], Manoranjan Kar[b]

[a]Department of Applied Physics, BIT, Mesra, Ranchi, Jharkhand, India
[b]Department of Physics, IIT, Patna, Bihar, India

Received 16 May 2013; received in revised form 20 May 2013; accepted 21 May 2013
Available online 28 May 2013

Abstract

Strontium calcium tungstates $(Sr_{1-x}Ca_x)WO_4$ crystals (with $x=0$; 0.1, 0.2, 0.3, 0.4, 0.5, 0.6,0.7, 0.8, 0.9 and 1.0) were prepared by the standard wet milling ceramic preparation method. X-ray diffraction (XRD), Fourier transform Raman (FT-Raman) and Fourier transform infrared (FT-IR) spectroscopic techniques indicate that all the crystals present a scheelite-type tetragonal structure without deleterious phases. FT-Raman spectra exhibited six Raman active modes in the range from 100 to 1000 cm^{-1}, while the FT-IR spectra present different infrared active modes for W–O within the wave number range from 500 to 1000 cm^{-1}. Optical properties were investigated by ultraviolet visible (UV–vis) absorption and photoluminescence (PL) measurements. UV–vis absorption measurements evidenced an increase in the values of the optical band gap (from 5.80 to 5.92 eV) with the increase of Ca into the $SrWO_4$ lattice. All compositions show broad blue PL emission at room temperature when excited with 250 nm wavelength. Dielectric constant, temperature coefficient of resonant frequency (τ_f) and quality factors were measured with the Hakkie–Coleman technique. The permittivity was found to increase with the increase in Ca content, in agreement with the Clausius–Mosotti relation. The value of τ_f was found to be −44.61 ppm/°C for $SrWO_4$ which increased to −19.69 ppm/°C for $CaWO_4$.

Keywords: Ceramics; Tungstate; Microwave dielectrics; Clausius–Mosotti relation

1. Introduction

Alkaline earth metal tungstates, AWO_4 (A=Ca,Sr, and Ba), are the members of an important inorganic materials family with a distinctive scheelite-type structure [1,2]. These compounds crystallize in $I4_1/a$ space group with four molecules in each crystallographic cell. The divalent A^{2+} and hexavalent W^{6+} atoms coordinate with eight and four O^{2-} atoms, respectively [3]. These materials have wide applications in various fields such as electro-optics, microwave ceramics, lasers and amplifiers [4]

Calcium and strontium tungstates from the scheelite family remain center of attraction for crystal growers, radiologists, material scientists and physicists due to their potential application in the field of electronic and opto-electronic industries. Calcium tungstate is the most widely used phosphor in industrial radiology and medical diagnosis [5–7], solid-state LASER action that gives 64% higher slope efficiency than Nd: YAG laser [8] storage applications [9] tunable fluorescence [10] sensor for dark matter search [11]and for the detection of γ- rays [12]. Strontium tungstate is also a very important member of the scheelite family. It is an efficient scintillator at low temperatures, and has gained a lot of interest due to the possibility of combining laser and Raman properties in the same media [13]. Despite the similar crystal structure, tungstates with scheelite crystal structure have substantially different luminescent properties. At room temperature $CaWO_4$ shows intense blue luminescence with microsecond decay, $PbWO_4$ shows weak nanosecond blue luminescence while $SrWO_4$ shows either blue or green luminescence emissions [14]. On the other hand the luminescence of $BaWO_4$ is almost undetectable. Hence these materials have attracted considerable attention for the development of new electro-optics devices.

A number of synthesis methods, including solid state reaction [15], electrochemical [16], micro-emulsion [17,18],

*Corresponding author. Tel.: +91 9471555277.
E-mail addresses: skrout@bitmesra.ac.in, drskrout@gmail.com (S.K. Rout).

0272-8842/$ - see front matter © 2013 Elsevier Ltd and Techna Group S.r.l. All rights reserved.
http://dx.doi.org/10.1016/j.ceramint.2013.05.084

hydrothermal [19], moltensalt [20], sono chemical [21],bio-membrane template [22], microwave-hydrothermal [23], and polymer template [24], have been employed to manipulate the shapes and sizes of AWO_4 (A=Ca, Sr, and Ba) micro and nanostructures. Among these methods, solution-based chemical synthetic methods play a key role in the design and production of fine ceramics. Furthermore, the use of solution chemistry can eliminate major problems, such as a long diffusion path, impurities and agglomeration, which result in products with improved homogeneity. Wet chemical methods have disadvantages, such as complicated synthetic steps, the use of expensive precursors, expensive equipments, high synthesis temperatures and long sintering times. On the other hand the solid-state reactions require excessive energy consumption. However solid-state, high temperature method is still industrially accepted for mass production due to its cost effectiveness [25].

The luminescent properties of single-crystal as well as polycrystalline $SrWO_4$ and $CaWO_4$ have been widely studied in the past. Wo et al. studied the thermodynamic properties and reported that enthalpies of formation for $MeWO_4$ (Me is Mg, Ca, Sr, Ba) increases with the increase of ionic radii of alkaline earth metal [26]. It means that scheelite $SrWO_4$ is more thermodynamically stable than $CaWO_4$. The relation between ionic parameters and intrinsic microwave dielectric properties has been investigated by IR spectrum study for the complex perovskite ceramics [27]. Ionic size, manifesting itself in tolerance factor (t), is found to be the most important parameter in controlling the intrinsic microwave dielectric properties. For $t>1$, W-site has too much room, resulting in an increasing of damping of the second mode involving W-site vibration. Damping could be minimized by changing the ionic size to fulfill, $t\sim1$. Based on the aforementioned consideration, we choose smaller sized Ca^{2+} for higher radii Sr^{2+} so as to reduce the tolerance factor.

On the other hand, $SrWO_4$ was reported to have negative-temperature coefficient of resonant frequency (τ_f) value (−55) [28], thus near zero τ_f value is expected to be tuned for the same by substituting a lower radii Ca^{2+} on Sr^{2+}site. The physical properties of these scheelites, those render them as an appropriately attractive material, are evidently and intimately-coupled with their unit cell dimension, crystallographic symmetry, as well as band structure. Hence, in this article, we seek to gain a fundamental understanding of how slight but controlled variations in the chemical composition of these scheelite materials may lead to favorable structure property correlations in these systems. The goal was to investigate the crystal structure, microstructure, microwave dielectric and optical properties of $Sr_{1-x}Ca_xWO_4$ prepared using the wet milling ceramics preparation technique and compare with previously reported distortions in WO_4 tetrahedra using Raman spectroscopy and photoluminescence measurements.

2. Experimental procedure

$Sr_{1-x}Ca_xWO_4$ ceramics were prepared using the solid state reaction method. Highly pure chemicals, strontium carbonate (99%, Himedia Chemicals), tungstan oxide (99%, Alfa Assar) and calcium carbonate (99%, Merck India Ltd.) were used. The stoichiometrically calculated reagents were thoroughly mixed in the liquid medium using agate mortar and pestle for 4 h.The obtained mixtures were dried and uni-axially pressed into pellets. The pellets were heat treated at 900 °C and 1300 °C at heating rates of 5 °C/min with an intermediate grinding for 4 h. The bulk density of the sintered samples was measured by Archimedes water immersion technique. The microstructures were examined using a scanning electron microscope (SEM, JEOL-6330F, JEOL, Japan). The pellets were crushed and structurally characterized by using PANAlytical X-pert pro MPD in Bragg–Brentano geometry with an X-Cellerator detector. XRD patterns were obtained using Cu Kα radiation in the 2θ range from 20° to 80° with a scanning rate of 0.02°/min and a step size of 0.017°. Raman studies were performed using STR500, Seki Technotron spectrometer with an excitation wavelength at 514.5 nm, from an Ar laser. Fourier-infrared (FT-IR) absorption spectrum was recorded by the standard KBr pellet technique using FT-IR spectrometer (IR-Prestige21,SHIMADZU, Japan). The optical band gap was calculated using UV–vis spectra recorded through a standard spectrophotometer (Lambda 35, PerkinElmer,) in the diffuse reflection mode. PL measurements of powders were performed on a Hitachi F-7000 fluorometer with a Xe lamp as the excitation light source at roomtemperature. The excitation wavelength was 240 nm. Microwave dielectric constant and unloaded Q values at microwave frequencies were measured using the TE01δ resonance mode using the Hakki–Coleman [29] dielectric resonator method as modified and improved by Courtney [30] in the frequency range 1–12 GHz. τ_f was calculated by measuring the resonant frequency in the temperature range from 30–70 °C at a step of 10 °C. These values were measured by inserting the cylindrical pellets in a shielding cavity connected to an Agilent PNA E8364B network analyzer in the transmission setup with a weak or moderate coupling [31,32].

3. Results and discussion

Fig. 1 shows the XRD pattern of $Sr_{1-x}Ca_xWO_4$ powders. All diffraction peaks shows single phase scheelite type tetragonal structure with space group $I4_1/a$. The diffraction patterns of all compositions show crystalline nature of the ceramics. No additional or intermediate phases were detected. This suggests the complete solubility of Ca in the $SrWO_4$ crystal lattice. The diffraction peaks are found shifted to higher 2θ position with an increase of Ca concentration suggesting decrease in cell volume. This decrease in cell volume is due to the smaller ionic radius of Ca^{2+} than that of Sr^{2+}.

Fig. 2 shows the composition dependency of absorption band positions derived from FT-IR spectra recorded in the region of 400–1500 cm^{-1}. In $SrWO_4$ the stretching vibration is detected at 411 cm^{-1}. However, Oh et al. [33] studied the composition within the wave number range from 480 to 4000 cm^{-1} and observed an absorption band at 831.57 cm^{-1}, assigned as an anti-symmetric stretching vibration. This band

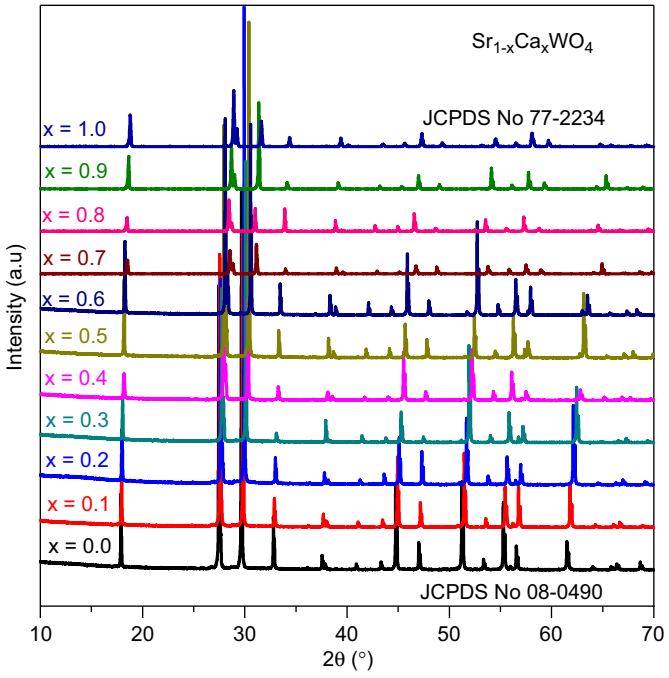

Fig. 1. XRD pattern of $Sr_{1-x}Ca_xWO_4$ powders recorded at room temperature. XRD patterns of $CaWO_4$ and $SrWO_4$ are in agreement with the JCPDS card no 08-0490 and 77-2234 respectively.

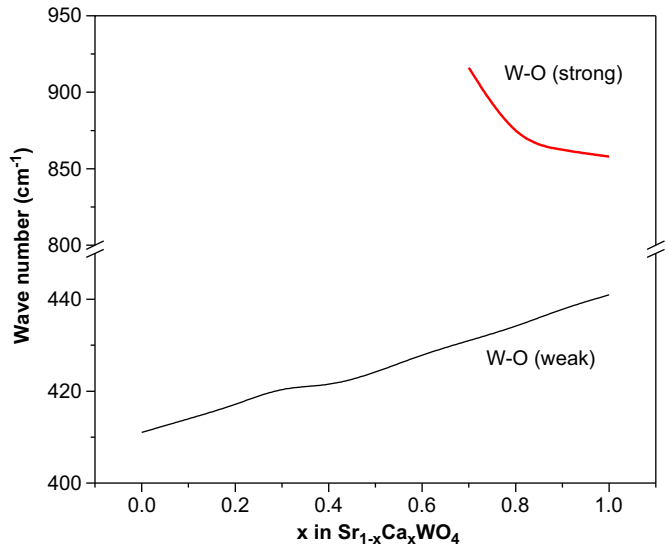

Fig. 2. Composition dependence of absorption band position derived from room temperature FTIT spectra.

is absent in the present $SrWO_4$ sample and remain absent upto $x=0.7$. The observed band at 411 cm^{-1} is designated as weak W–O symmetric stretch in the $[WO4]^{2-}$ tetrahedron. This band position was found shifting toward higher energy side with increase in the Ca content. This shifting may be due to increase in the W–O bond strength resulted due to strengthening of Sr/Ca–O band. This bond strengthening occurs may be due to reduction of bond length between metal cation and oxygen (Sr/Ca–O), by the substitution of smaller radii Ca in place of Sr. The composition with $x=0.7$ shows additional strong stretching vibrations at 916 cm^{-1} and found shifting toward lower wave number side with increase in the Ca Content. The observed band positions for $CaWO_4$ are quite similar with the literature reported for $CaWO_4$ prepared by a microwave irradiation technique [34]. In general our FT-IR result is analogous to the result reported by Zhang etal. [35]

Fig. 3 shows the room temperature Raman spectra of the $Sr_{1-x}Ca_xWO_4$ ceramics. The Raman spectra are able to predict the degree of structural order–disorder at short range in the materials. The $[WO_4]$ molecular groups with strong covalent bond W–O are peculiar to the tungstates. Due to weak coupling between the $[WO_4]$ molecular groups and the Ca^{2+} or Sr^{2+} cations, the vibrational modes observed in Raman spectra of $Sr_{1-x}Ca_xWO_4$. The group theory calculation presents 26 different vibration for $Sr_{1-x}Ca_xWO_4$, which is represented by following equation.

$$\Gamma = 3A_g + 5A_u + 5B_g + 3B_u + 5E_g + 5E_u$$

where all vibration (A_g, B_g, and E_g) are Raman-active. A and B modes are non-degenerate, whereas E modes are doubly degenerate. The subscribed 'g' and 'u' for even and odd, respectively, indicate the parity under inversion in centro-symmetric crystals. One A_u and E_u correspond to the zero frequency of acoustic modes, the others are optic modes. In scheelites, the first member of the pairs (g) is a Raman-active mode and the second member (u) is active only in infrared (IR), except for the Bu silent modes that are not IR active. So, we expect 13 zone-center Raman-active modes in $Sr_{1-x}Ca_xWO_4$ as presented in following equation.

$$\Gamma = 3A_g + 5B_g + 5E_g$$

This leads to seven internal modes namely (a) the stretching vibrations: $\nu_1(A_g)$, $\nu_2(B_g)$, and $\nu_3(E_g)$ and (b) bending modes: ν_2 (A_g), $\nu_2(B_g)$, $\nu_4(B_g)$ and $\nu_4(E_g)$. There are six external modes

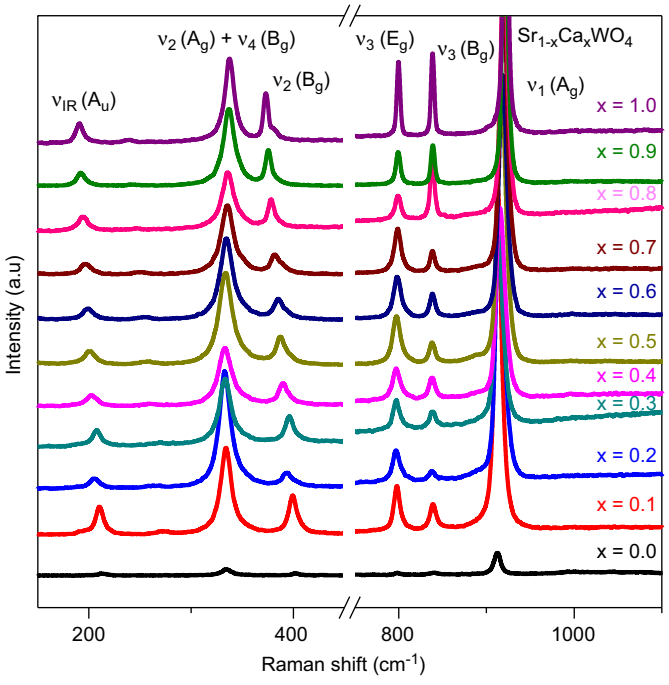

Fig. 3. Room temperature Raman spectra of $Sr_{1-x}Ca_xWO_4$ ceramics.

namely two rotational modes of A_g and E_g symmetry and four translational modes namely $2B_g$ and $2E_g$ [23,36]. The external modes are called lattice phonon which correspond to the motion of Sr^{2+}or Ca^{2+}cations and the rigid molecular units [23].The internal modes belong to the vibration inside $[WO_4]^{2-}$ tetrahedrons have cubic point symmetry T_d [36]. The stronger Raman-active vibration modes indicate a strong interaction between the ions, which mainly arise due to the stretching and bending vibration of the shorter metal–oxygen bonds within the anionic groups [37]. Only six Raman-active modes were detected in the ceramics prepared using the solid state reaction route within the frequency range 50–1000 cm^{-1} and are shown in Fig. 3. According to literature [38,39], the scheelite structure has been shown to be one of the few for which the correlation splitting of the internal modes has been observed. This results in ν_1: A_g(R)+B_u (inactive/silent), ν_2: A_g+B_g(R)+A_u(ir)+B_u, ν_3, ν_4: B_g+E_g(R)+A_u(ir)+E_u(ir). The spectrum for all compositions in the present study contains, $2A_g$ vibrations, $3B_g$ and $1E_g$ mode. The typical frequencies quoted for $[WO_4]^{2-}$ regular octahedron and the frequencies observed in the present study are listed in Table 1.

The $\nu_1(A_g)$ band is observed at 911 cm^{-1} for $CaWO_4$ while same band is observed at 921 cm^{-1} for $SrWO_4$. The corresponding $\nu_1(B_u)$ vibration is not observed in any composition because this $\nu_1(B_u)$ vibration is inactive or a silent mode. However, Frost et al. [40] have observed a minor band around 894 cm^{-1} in scheelite structure materials and explained that may be due to strain in the crystal causing activation of this silent band. The $\nu_2(A_g)$ vibration is observed as a strong band at around 332 cm^{-1} for $CaWO_4$ and at 337 cm^{-1} for $SrWO_4$. $CaWO_4$ showed a weak $\nu_2(B_g)$ at 400 cm^{-1} while 374 cm^{-1} for $SrWO_4$ and the $\nu_2(B_u)$, which is expected at 428 cm^{-1} as a very weak bond, is absent. The $\nu_3(B_g)$ vibration is located around 840 cm^{-1} for $CaWO_4$ while same band is observed at 838 cm^{-1} for $SrWO_4$. The $\nu_3(E_g)$ is located around 800 cm^{-1} for all compositions. Finally, the $\nu_4(B_g)$ vibration is found completely overlapping with the $\nu_2(A_g)$ vibration of all compositions. The $\nu_4(E_g)$ mode is absent in the present spectra although [41] reports this band at 409 cm^{-1}. The bands at around 186–189 cm^{-1} have not been previously reported. This band may be the equivalent of the infrared active $\nu_4(A_u)$ activated due to strain in the crystal. However, Daturi et al. [42] assign a similar band at 273 cm^{-1} as a Raman active $\nu(B_g)$ mode for scheelite type $CdMoO_4$ and also bands at 193 cm^{-1} assigned to translational modes of the WO_4 group.

Fig. 4 shows the band gap energy as a function of Sr content. The equation proposed by Wood and Tauc [44] was used to estimate the optical band-gap from UV–vis spectra. According to these authors, the optical band-gap energy is related with absorbance and photon energy by the following equation; $h\upsilon\alpha\ \alpha\ (h\upsilon - E_g)^{1/2}$, where α is the absorbance, h is the Planck constant, υ is the frequency and E_g is the optical band gap. The E_g value was evaluated by extrapolating the linear portion of the curve. The value of direct transition band gap of $CaWO_4$ was found to be 5.92 eV. Similar value of band gap of crystalline $CaWO_4$ film was observed by Refs. [45,46] which was 5.27 and 5.4 eV respectively. As illustrated in Fig. 4 the

Table 1
Raman active frequencies quoted in literature and observed in the present for $Sr_{1-x}Ca_xWO_4$ ceramics.

$SrWO_4$ in [43]	x in $Sr_{1-x}Ca_xWO_4$ (present work)										$CaWO_4$ in [34]	Mode symmetry
	0.0	0.1	0.2	0.3	0.4	0.5	0.6	0.7	0.8	0.9	1.0		
925	921	921	921	919	917	918	915	913	915	913	911	912	$\nu_1(A_g)$
839	838	838	838	838	836	838	838	838	836	838	840	838	$\nu_3(B_g)$
797	800	798	798	798	796	797	796	796	796	797	797	797	$\nu_3(E_g)$
370	374	375	377	382	384	388	392	395	394	399	400	400	$\nu_2(B_g)$
334	337	337	335	335	333	332	331	333	333	332	332	332	$\nu_2(A_g)+\nu_4(B_g)$
187	190	192	194	196	198	199	202	206	204	210	210	210	ν_{fr}

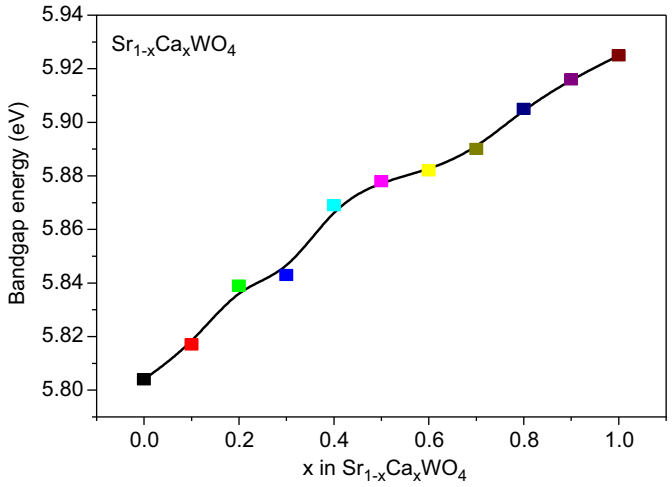

Fig. 4. Composition dependence of band gap energy derived from UV–vis absorption spectra.

band gap energy increases as Cacontain in the composition increases [47]. It has been reported that E_g is associated with the presence of intermediary energy levels within the band-gap of the materials [48]. These energy levels are also dependent of the degree of structural order–disorder in the lattice. Therefore, the increase in structural organization in the lattice leads to formation of intermediary energy levels and consequently increases the band gap. The E_g values can also be related to the other factors such as; preparation method, processing time and temperature, particles shape and morphology. These factors affect the different structural organizations like oxygen vacancies, bond distortions leading to affect the formation of intermediary energy levels within the band gap. The value of band gap for $SrWO_4$ was found to be 5.80 eV. This value reported in literature as 4.5 eV for $SrWO_4$ powder prepared using the polymeric precursor method [49], 4.49 eV for the crystal prepared using double decomposition flux reaction [47], 4.43 for the powder prepared using microwave hydrothermal route [50] and 3.90 eV for the powder prepared using solid state reaction route heated at 1300 °C [51]. Our observed band gap value for $SrWO_4$ suggests that the sample has very less defect and comparable to the samples prepared using other chemical route. The observed value of band gap for end members of the series are in good agreement with literature and systematic change with composition suggest that all samples are structurally ordered at long and short range, in agreement with XRD and Raman study.

Fig. 5 presents the photo luminescent emission spectrum of the $Sr_{1-x}Ca_xWO_4$ ceramics prepared using solid state reaction route.The Gaussian nature of the spectra indicates that the electronic levels corresponding to relaxed excited state of an emission center belong to a degenerate excited state influenced by some perturbation, e.g. a local low symmetry crystal field [52]. Such emission peaks can be explained by the influence of the Jahn–Teller effect [53] on the degenerated excited state of $[WO_4]^{2-}$ tetrahedron.With excitation at 250 nm, the spectra show symmetric peaks spread between 350 and 550 nm. The broad nature of spectra suggests involvement of several energy state within the band gap. Therefore to have qualitative information deconvolution was performed using the multipeak Gaussian fit to the emission spectra of ceramics. All spectra show, emission is composed of two types of groups.The first major peaks are located at the blue wavelength 409–420 nm, the second peaks are in between 456 and 480 nm.It is generally assumed that the measured emission spectra of metal tungstates are mainly attributed to the charge–transfer transitions within the $[WO_4]^{2-}$ complex between the last fully occupied t_2 orbital and the first empty e orbital [54,55]. More detail about the charge transfer on the basis of hybridization of the $[WO4]^{2-}$ anionic tetrahedrons is explained in the literature [50,56]. The intensity of the emission spectra gradually increases with increase in Ca content. As discussed in the previous section that the band gap of $CaWO_4$ is higher than that of $SrWO_4$. So $CaWO_4$ can absorb higher energies than $SrWO_4$. Hence, the higher emission intensity can be explained on the basis of optical band gap energy. The different intensities may also be resulted from the different sizes and surface properties of ceramics. The position of the emission peaks are not considerably altered, implying that the energy band gap relating to the blue emission is not highly affected by the variation in chemical composition.

Microwave dielectric measurements were performed using N5230A (Agilent Technologies, USA) Vector Network Analyzer in a TE_{011}. The dielectric constant (ε_r) were measured using the [29] dielectric resonator method as modified and improved by Courtney [30]. The TE_{011} mode is widely used in materials property characterization because in this mode there is no current crossing the dielectric and the conducting plates, so possible air gaps between the dielectric and the conducting plates have no effects on resonance properties of this mode [57]. The theoretical model is properly described for the

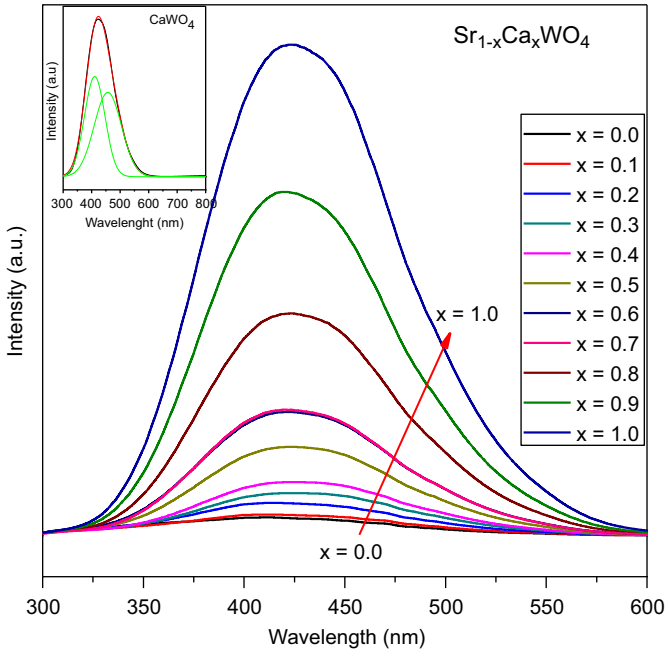

Fig. 5. Room temperature photoluminescence emission spectra of $Sr_{1-x}Ca_xWO_4$ ceramics excited with 250 nm. The inset shows a representative multi peak Gaussian fit to the emission spectra of $CaWO_4$.

configuration mentioned by Courtney and as modified from Kobayashi and Tanaka [58]. The TE_{011} resonance mode has been found most suitable for the real part of the relative dielectric constant (ε_r), and a gain/loss factor ($\tan\delta$) of the specimen was obtained from the measured resonance frequency (f_1) and unloaded quality factor (Q_0) for the TE_{011} resonance mode. The relative dielectric constant and loss factors were calculated from the following formula [29]

$$\varepsilon_r = 1 + \left(\frac{c}{\pi D f_1}\right)(\alpha_1^2 + \beta_1^2) \quad (1)$$

where c is the velocity of light, α_1 is given by the mode chart [58] and β_1 is obtained from the resonance frequency (f_1) and the sample dimension. The $\tan\delta$ is given by Hakki–Coleman [29] as described in Eq. (2)

$$\tan\delta = \frac{A}{Q_u} - BR_S \quad (2)$$

where:

$$A = 1 + \frac{W}{\varepsilon_r} \quad (3)$$

$$B = \left(\frac{l\lambda}{2L}\right)^3 \frac{1+W}{30\pi^2\varepsilon_r l} \quad (4)$$

$$W = \frac{J_1^2(\alpha_1)}{K_1^2(\beta_1)} \frac{K_0(\beta_1)K_2(\beta_1) - K_1^2(\beta_1)}{J_1^2(\alpha_1) - J_0(\alpha_1)J_2(\alpha_1)} \quad (5)$$

$$R_s = \sqrt{\frac{\pi f_1 \mu}{\sigma}} \quad (6)$$

The function W is the ratio of electric field energy stored on the outside of the rod to the energy inside the rod. λ is the free-space wavelength and L is the length of the dielectric specimen. σ is the conductivity of the shorting plate, and Q_0 is the unloaded quality factor of the dielectric resonator. If the dielectric material is isotropic then the characteristic equation for such a resonance structure for the TE_{011} mode is given by Eq. (7):

$$\alpha\frac{J_0(\alpha)}{J_1(\alpha)} = -\beta\frac{K_0(\beta)}{K_1(\beta)} \quad (7)$$

where $J_0(\alpha)$ and $J_1(\alpha)$ are the Bessel functions of the first kind of order zero and one, respectively. $K_0(\beta)$ and $K_1(\beta)$ are the modified Bessel functions of the second kind of orders zero and one, respectively. Kobayashi and Katoh [59] described a method for the experimental determination of R_s which employs two rod samples cut from the same dielectric rod with equal diameters but different lengths. The expression of R_s is given by:

$$R_s = 30\pi^2\left(\frac{2L}{l\lambda}\right)^3 \frac{\varepsilon_r + W}{1+W}\frac{1}{l-1}\left(\frac{1}{Q_{01}} - \frac{1}{Q_{0l}}\right) \quad (8)$$

Then substitution of Eq. (8) into Eq. (2) yields:

$$\tan\delta = \frac{A}{l-1}\left(\frac{l}{Q_{0l}} - \frac{1}{Q_{01}}\right) \quad (9)$$

Table 2
The values of calculated molar volume, calculated permittivity (ε_r^s), apparent porosity, observed permittivity(ε_{obs}), permittivity after porosity correction (ε_{corr}), temperature coefficient of resonant frequency (τ_f), quality factor and dielectric loss tangent of $Sr_{1-x}Ca_xWO_4$.

x in SCW	Molar volume	α_D	ε_r^s	Apparent porosity	ε_{obs}	ε_{corr}	τ_f (ppm/°C)	$Q\times f$ (GHz)	$\tan\delta$
$x=0.0$	87.72	15.48	9.50	0.0690	8.44	9.32	−44.61	6,907.29	1.12×10^{-3}
$x=0.1$	86.63	15.37	9.68	0.0650	8.57	9.41	−39.42	18,208.02	4.46×10^{-4}
$x=0.2$	86.02	15.26	9.67	0.0598	8.69	9.47	−38.58	10,697.54	7.78×10^{-4}
$x=0.3$	85.31	15.15	9.71	0.0403	8.99	9.54	−26.17	4,406.98	1.93×10^{-3}
$x=0.4$	84.56	15.04	9.76	0.0396	9.08	9.61	−25.97	5,240.91	1.57×10^{-3}
$x=0.5$	81.51	14.94	10.91	0.0460	10.03	10.72	−25.94	5,735.50	1.44×10^{-3}
$x=0.6$	80.35	14.83	11.22	0.0388	10.45	11.08	−25.88	7,248.16	1.41×10^{-3}
$x=0.7$	79.54	14.72	11.34	0.0427	10.62	11.31	−25.78	10,385.06	7.84×10^{-4}
$x=0.8$	78.80	14.61	11.43	0.0371	10.78	11.38	−25.65	83,543.16	1.05×10^{-3}
$x=0.9$	77.93	14.50	11.59	0.0327	10.89	11.42	−25.46	13,485.63	5.96×10^{-4}
$x=1.0$	77.43	14.40	11.57	0.0417	10.94	11.63	−19.69	8,786.09	9.26×10^{-4}

This calculation facilitates the precise measurement of (tan δ). Temperature coefficients of the dielectric resonator were measured using a temperature controlled hot plate enclosure with an invar cavity in the temperature range from 40 °C to 70 °C using Eq. (10)

$$\tau_f = \left(\frac{1}{f}\right)\left(\frac{\Delta f}{\Delta T}\right) \quad (10)$$

where $\Delta f/\Delta T$ is the resonance frequency change with respect to temperature.

According to Shannon [60] the molecular polarizibilities of complex substances can be broken up into the polarizibilities of constituent ions which can be estimated from the following equation.

$$\alpha(AWO_4) = \alpha(A^{2+}) + \alpha(W^{6+}) + 4\alpha(O^{2-}) \quad (11)$$

where α is the polarizability. The dielectric constants of AWO_4 compounds could be calculated with the polarizability from Shannon's suggestion and the Clausius–Mosotti relation:

$$\varepsilon_s = \left(\frac{3V_m + 8\pi\alpha_D}{3V_m - 4\pi\alpha_D}\right) \quad (12)$$

where V_m is the molar volume. Molar volume of AWO_4 can be calculated with the unit cell parameters determined from the diffraction pattern, and the values of molar volume are shown in Table 2. The dielectric constant of AWO4 was calculated with 3.2 for the mean value of polarizability of W^{6+}. The calculated and observed permittivity after porosity correction of $Sr_{1-x}Ca_xWO_4$ ceramics are shown in Table 2. The porosity correction was applied as per the equation, $\varepsilon_r = \varepsilon^{obs}(1+1.5\,P)$, where P is porosity. The calculated and observed permittivity after porosity correction showed good agreement. Pullar et al. [61], reported similar values of permittivity for different wolframite and scheelite structured ceramics sintered at 1200 °C. The observed values of τ_f for end compositions are higher than those reported by Yoon et al., [28] may be due to uniform grain growth of the ceramics and higher bulk density. One can see the apparently random variation in quality factor with x content in the samples. This may be due to variation in the apparent porosity of the samples.

4. Conclusion

Strontium calcium tungstates ($Sr_{1-x}Ca_xWO_4$) crystals (with x=0.0, 0.1, 0.2, 0.3, 0.4, 0.5, 0.6, 0.7, 0.8, 0.9, and 1.0) were prepared by the standard wet milling ceramic preparation method. The structural characterization showed formation of single phase scheelite tetragonal structure without evidence of any secondary phase. FT-Raman spectra exhibited six Raman active modes within the range from 100 to 1000 cm^{-1}, while the FT-IR spectra present different infrared active modes for W–O within the wave number range from 500 to 1000 cm^{-1}. Optical properties were investigated by ultraviolent visible (UV–vis) absorption spectroscopy showed an increase in band gap energy from 5.80 to 5.92 eV. All compositions show broad blue PL emission at room temperature when excited with 250 nm wavelength. Dielectric constant, temperature coefficient of resonant frequency (τ_f) and quality factors were measured with Hakkie–Coleman technique. The permittivity increases with increase in Ca content, in consistent with the Clausius–Mosotti relation. The value of τ_f was found to be −44.61 ppm/°C for $SrWO_4$ which increased to −19.69 ppm/°C for $CaWO_4$.

Acknowledgments

Authors are pleased to acknowledge the Central Instrumentation Facility, Birla Institute of Technology, Mesra for providing the experimental facilities for this work. The corresponding author (SKR) gratefully acknowledges Department of Science and Technology, Government of India, New Delhi, for providing financial support through a fast track research grant no. CS-037/2013.

References

[1] H.W. Liao, Y.F Wang, Y.M Liu, Y.D. Li, Y.T. Qian, Hydrothermal preparation and characterization of luminescent $CdWO_4$ nanorods, Chemistry of Materials 12 (10) (2000) 2819–2821.
[2] Qiao Zhang, Wei-Tang Yao, Xianyu Chen, Liwei Zhu, Yibing Fu, Guobin Zhang, Liusi Sheng, Shu-Hong Yu, Nearly monodisperse tungstate MWO4 microspheres (M=Pb, Ca): surfactant-assisted solution synthesis and optical properties, Crystal Growth & Design 7 (8) (2007) 1423–1431.
[3] E. Gurman, E. Daniels, J.S. King, Crystal structure refinement of $SrMoO_4$, $SrWO_4$, $CaMoO_4$, and $BaWO_4$ by neutron diffraction, Journal of Chemical Physics 55 (1971) 1093.
[4] S.D. Colson, K.N. Wong, Overtone spectra of crystalline $CaWO_4$: vibrational exciton density-of-states functions, Chemical Physics 69 (1982) 223–228.
[5] M.V. Nazarov, B.S. Tsukerblat, E.-J. Popovici, D.Y. Jeon, Optical lines in europium–terbium double activated calcium tungstate phosphor, Physics Letters A 330 (3–4) (2004) 291–298.
[6] G.E. Gilakoumakis, I.E. Lagaris, A theoretical model for the cathodoluminescence of granular phosphor screens, Journal of Applied Physics 64 (1988) 5106.
[7] L.H. Brixner, New X-ray phosphor, Materials Chemistry and Physics 16 (3–4) (1987) 253–281.
[8] N. Faure, C. Borel, M. Couchaud, G. Basset, R. Templier, C. Wyon, Optical properties and laser performance of neodymium doped scheelites $CaWO_4$ and $NaGd(WO_4)_2$, Applied Physics B 63 (1996) 593.
[9] A. Caprez, P. Meyer, P. Mikhail, J. Hulliger, New host-lattices for hyperfine optical hole burning: materials of low nuclear spin moment, Materials Research Bulletin 32 (1997) 1045–1054.
[10] M.V. Nazarov, D.Y. Jeon, J.H. Kang, E.J. Popovici, L.E. Muresan, M. V. Zamoryanskaya, B.S. Tsukerblat, Luminescence properties of europium–terbium double activated calcium tungstate phosphor, Solid State Communications 131 (2004) 307–311.
[11] S. Cebrian, N. Coron, G. Dambier, P. de Marcillac, E. Garcia, I. G. Irastorza, J. Leblanc, A. Morales, J. Morales, A.Ortiz de Solorzano, J. Puimedon, M.L. Sarsa, J.A. Villar, First underground light versus heat discrimination for dark matter search, Physics Letters B 563 (2003) 48–52.
[12] F. Petricca, G. Angloher, C. Cozzini, T. Frank, D. Hauff, J. Ninkovic, F. Probst, W. Seidel, S. Uchaikin, Light detector development for CRESST II, Nuclear Instruments and Methods in Physics Research Section A 520 (2004) 193.
[13] L.I. Ivleva, T.T. Basiev, I.S. Voronina, P.G. Zverev, V.V. Osiko, N. M. Polozkov, $SrWO_4:Nd^{3+}$—new material for multifunctional lasers, Optical Materials 23 (2003) 439.

[14] Z. Lou, M. Cocivera, Materials Research Bulletin 37 (2002) 1573 and L. Chen, Y. Gao, Fabrication of luminescent $SrWO_4$ thin films by a novel electrochemical method, Materials Research Bulletin 42 (2007) 1823–1830.
[15] Z. Shan, Y. Wang, H. Ding, F. Huang, Structure-dependent photocatalytic activities of MWO_4 (M=Ca, Sr, Ba), Journal of Molecular Catalysis A 302 (2009) 54–58.
[16] Hao Zhuang, Zhenxing Yue, Siqin Meng, Fei Zhao, Longtu Li, Low-temperature sintering and microwave dielectric properties of $Ba_3(VO_4)_2$–$BaWO_4$ ceramic composites, Journal of the American Ceramic Society 91 (2008))3738–3741.
[17] Fen Zhang, Matthew Y. Sfeir, James A. Misewich, Stanislaus S. Wong, Room-temperature preparation, characterization, and photoluminescence measurements of solid solutions of various compositionally-defined single-crystalline alkaline-earth-metal tungstate nanorods, Chemistry of Materials 20 (2008) 5500–5512.
[18] J. He, M. Han, X. Shen, Z. Xu, Crystal hierarchically splitting in growth of $BaWO_4$ in positive cat–anionic microemulsion, Journal of Crystal Growth 310 (2008) 4581.
[19] J. Liao, B. Qiu, H. Wen, J. Chen, W. You, L. Liu, Synthesis process and luminescence properties of Tm^{3+} in AWO_4 (A=Ca, Sr, Ba) blue phosphors, Journal of Alloys and Compounds 487 (2009) 758.
[20] Xiaohui Jiang, Junfeng Ma, Yan Yao, Yong Sun, Zhensen Liu, Yang Ren, Jun Liu, Botao Lin, Low-temperature synthesis of $SrWO_4$-nano-particles by a molten salt method, Ceramics International 35 (2009))3525.
[21] Titipun Thongtem, Anukorn Phuruangrat, Somchai Thongtem, Characterization of $MeWO_4$ (Me=Ba, Sr and Ca) nanocrystallines prepared by sonochemical method, Applied Surface Science 254 (2008) 7581–7585.
[22] F. QDong, Q.S. Wu, Y.P. Ding, Morphology-controlled synthesis of $BaWO_4$ crystals via biominmetic SLM system, Journal of Alloys and Compounds 476 (2009) 571–576.
[23] L.S. Cavalcante, J.C. Sczancoski, J.W.M. Espinosa, J.A. Varela, P. S. Pizani, E. Longo, Photoluminescent behavior of $BaWO_4$ powders processed in microwave-hydrothermal, Journal of Alloys and Compounds 474 (2009) 195.
[24] Z. Luo, H. Li, J. Xia, W. Zhu, J. Guo, B. Zhang, Microwave-assisted synthesis of barium tungstate nanosheets and nanobelts by using polymer PVP micelle as templates, Materials Letters 61 (2007) 1845.
[25] Chang Sung Lim, Solid-state metathetic synthesis of $BaMO_4$ (M=W, Mo) assisted by microwave irradiation, Journal of Ceramic Processing Research 12 (5) (2011) 544–548.
[26] Jia Yin Wo, Jian Jiang Bian, Structure stability and microwave dielectric properties of double perovskite ceramics—$Ba_2Mg_{1-x}Ca_xWO_6$ ($0.0 \le x \le 0.15$), Ceramics International 38 (2012) 3217–3225.
[27] R. Zurmuhlen, J. Petzelt, S. Kamba, V.V. Vooitsekhovskii, E. Colla, N. Setter, Dielectric spectroscopy of $Ba(B_{1/2}'B_{1/2}'')O_3$ complex perovskite ceramics: COrrelations between ionic parameters and microwave dielectric properties. I. Infrared reflectivity study (10^{12}–10^{14} Hz), Journal of Applied Physics 77 (10) (1995) 5341–5350.
[28] S.H. Yoon, D.W. Kim, S.Y. Cho, K.S. Hong, Investigation of the relations between structure and microwave dielectric properties of divalent metal tungstate compounds, Journal of the European Ceramic Society 26 (2006) 2051–2054.
[29] B.W. Hakki, P.D. Coleman, A dielectric resonator method of measuring inductive in the millimeter range, IRE Transactions on Microwave Theory and Techniques 8 (1960) 402–410.
[30] W.E. Courtney, Analysis and evaluation of a method of measuring the complex permittivity and permeability of microwave insulators, IEEE Transactions on Microwave Theory and Techniques 18 (1970) 476–485.
[31] J. Krupka, K. Derzakowski, B. Riddle, J. Baker–Jarvis, A dielectric resonator for measurements of complex permittivity of low loss dielectric materials as a function of temperature, Measurement Science and Technology 9 (1998) 1751–1756.
[32] J. Krupka, Frequency domain complex permittivity measurements at microwave frequencies, Measurement Science and Technology 17 (2006) R55–R70.
[33] Won-Chun Oh, Jong Geun Choi, Chong Yeon Park, Chang Sung Lim, Microwave-assisted synthesis of Ag incorporated $SrWO_4$/zeolite composites by a solid-state metathetic route, Journal of Ceramic Processing Research 12 (4) (2011) 435–438.
[34] A. Phuruangrat, T. Thongtem, S. Thongte, Synthesis, characterization and photoluminescence of nanocrystalline calcium tungstae, Journal of Experimental Nanoscience 5 (3) (2010) 236–270.
[35] G. Zhang, R. Jia, Q. Wu, Preparation structural and optical properties of AWO_4 (A=Ca, Ba, Sr) nanofilms, Materials Science and Engineering: B 128 (2006) 254–259.
[36] T.T. Basiev, A.A. Sobol, Yu.K. Voronko, P.G. Zverev, Spontaneous Raman spectroscopy of tungstate and molybdate crystals for Raman lasers, Optical Materials 15 (2000) 205–216.
[37] Z.C. Ling, H.R. Xia, D.G. Ran, F.Q. Liu, S.Q. Sun, J.D. Fan, H.J. Zhang, J.Y. Wang, L.L. Yu, Lattice vibration spectra and thermal properties of $SrWO_4$ single crystal, Chemical Physics Letters 85 (2006) 426.
[38] P. Cerny, H. Jelinkova, P.G. Zverev, T.T. Basiev, Solid state lasers with Raman frequency conversion, Progress in Quantum Electronics 28 (2004) 113.
[39] D. Rangappa, T. Fujiwara, M. Yoshimura, Synthesis of highly crystallized $BaWO_4$ film by chemical reaction method at room temperature, Solid State Sciences 8 (2006) 1074–1078.
[40] R. Frost, L. Duong, M. Weier, Raman microscopy of selected tungstate minerals, Spectrochimica Acta Part A: Molecular and Biomolecular Spectroscopy 60 (8–9) (2004) 1853–1859.
[41] S.D. Ross, Inorganic Infrared and Raman Spectra (European Chemistry Series)1972.
[42] M. Daturi, G. Busca, M.M. Borel, A. Leclaire, P. Piaggio, Vibrational and XRD study of the system $CdWO_4$–$CdMoO_4$, Journal of Physical Chemistry B101 (1997) 4358.
[43] S.P.S. Porto, J.F. Scott, Raman spectra of $CaWO_4$, $SrWO_4$, $CaMoO_4$ and $SrMoO_4$, Physical Review 157 (1967) 716.
[44] D.L. Wood, J. Tauc, Weak absorption tails in amorphous semiconductors, Physical Review B 5 (1972) 3144.
[45] N. Sainto, A. Kudo, T. Sakata, Synthesis of tungstate thin films and their optical properties, Bulletin of the Chemical Society of Japan 69 (1996) 1241.
[46] M.A.M.A Maurera, A.G Souza, L.E.B Soledade, F.M. Pontes, E. Longo, E.R. Leite, J.A. Varela, Microstructural and optical characterization of $CaWO_4$ and $SrWO_4$ thin films prepared by a chemical solution method, Materials Letters 58 (2004) 727–732.
[47] S.K. Arora, B. Chudasama, Crystallization and optical properties of $CaWO_4$ and $SrWO_4$, Crystal Research and Technology 41 (2006) 1089.
[48] J.C. Sczancoski, L.S. Cavalcante, M.R. Joya, J.A. Varela, P.S. Pizani, E. Longo, $SrMoO_4$ powders processed in microwave-hydrothermal: synthesis, characterization and optical properties, Chemical Engineering Journal 140 (2008) 632.
[49] M. Anicete-Santos, F.C. Picon, M.T. Escote, E.R. Leite, P.S. Pizani, J. A. Varela, E. Longo, Room-temperature photoluminescence in structurally disordered $SrWO_4$, Applied Physics Letters 88 (2006) 2119131.
[50] J.C. Sczancoski, L.S. Cavalcante, M.R. Joya, J.W.M. Espinosa, P. S. Pizani, J.A. Varela, E. Longo, Synthesis growth process and photoluminescence properties of $SrWO_4$ powders, Journal of Colloid and Interface Science 330 (2009) 227–236.
[51] H. Eng, P.W. Barnes, B.M. Auer, P.M. Woodward, Investigations of the electronic structure of d^0 transition metal oxides belonging to the perovskite family, Journal of Solid State Chemistry 175 (2003) 94–109.
[52] K. Polak, M. Nikl, K. Nitsch, M. Kobayashi, M. Ishii, Y. Usuki, O. Jarolimek, The blue luminescence of $PbWO_4$ single crystals, Journal of Luminescence 72–74 (1997) 781–783.
[53] J.V. Tol, J.H. Van Der Waals, The lowest triplet state of luminescent scheelites: a study of the MoO_4^{2-} ion by electron paramagnetic resonance with optical detection, Molecular Physics 88 (1996) 803–820.
[54] G.Y. Hong, B.S. Jeon, Y.K. Yoo, J.S. Yoo, Photoluminescence characteristics of spherical Y_2O_3: Eu phosphors by aerosol pyrolysis, Journal of the Electrochemical Society, 148, H161–H166.
[55] R. Grasser, A Scharmann, Luminescent sites in $CaWO_4$ and $CaWO_4$:Pb crystals, Journal of Luminescence 12–13 (1976) 473.
[56] T. Thongtem, A. Phuruangrat, S. Thongtem, Journal of Ceramic Processing Research 9 (3) (2008) 258–261.

[57] L.F. Chen, C.K. Ong, C.P. Neo, V.V. Varadan, V.K. Varadan, Microwave Electronics: Measurement and Materials Characterization (2004) 315.
[58] Y. Kobayashi, S. Tanaka, Resonant modes ofa dielectric rod resonator short circuited at both ends by parallel conducting planes, IEEE Transactions on Microwave Theory and Techniques 28 (1980) 1077.
[59] Y. Kobayashi, M. Katoh, Microwave measurement of dielectric properties of low–loss materials by the dielectric rod resonator method, IEEE Transactions on Microwave Theory and Techniques 33 (1985).
[60] R.D. Shannon, Dielectric polarizabilities of ions in oxides and fluorides, Journal of Applied Physics 73 (1993) 348–366.
[61] R.C. Pullar, S. Farrah, N.McN. Alford, $MgWO_4$, $ZnWO_4$, $NiWO_4$ and $CoWO_4$ microwave dielectric ceramics, Journal of the European Ceramic Society 27 (2007) 1059–1063.